ELSEVIER

Nuclear Instruments and Methods in Physics Research A 412 (1998) 254–264

NUCLEAR INSTRUMENTS & METHODS IN PHYSICS RESEARCH Section A

The optical properties of the BigBite spectrometer at NIKHEF

D.J.J. de Lange[a], H.P. Blok[a,b], D.J. Boersma[a,c], T. Botto[a], P. Heimberg[a,b], D.W. Higinbotham[d], I. Passchier[a], M.J.M. van Sambeek[a,b], E. Six[e], M.F.M. Steenbakkers[a,b], J.J.M. Steijger[a,*], H. de Vries[a]

[a] *NIKHEF, P.O. Box 41882, 1009 DB Amsterdam, The Netherlands*
[b] *Department of Physics and Astronomy, Vrije Universiteit, de Boelelaan 1081, NL-1081 HV Amsterdam, The Netherlands*
[c] *Universiteit Utrecht, P.O. Box 80.000, NL-3508 TA Utrecht, The Netherlands*
[d] *University of Virginia, Charlottesville, VA 22901, USA*
[e] *Department of Physics, Arizona State University, Tempe, AZ 85281, USA*

Received 24 February 1998; accepted 6 March 1998

Abstract

The optical properties of the BigBite spectrometer currently in use at the Internal Target Facility of the AmPS ring at NIKHEF have been determined. The spectrometer, which consists of a single dipole magnet, combines a large solid angle with a large momentum acceptance. The track of a particle is determined from the information of two sets of drift chambers behind the magnet. Tracing this track through the magnetic field to the target yields the position of the scattering vertex and the size and direction of the momentum vector of the scattered particle at the target position. These quantities are calculated using an analytical approximation of the spectrometer, followed by a refinement with the matrix method. The σ-resolutions of the reconstruction for 600 MeV electrons are 3 mrad for the angles, 3.2 mm for the vertex position, and 8.4×10^{-3} for $\delta p/p$.

PACS: 29.30.Aj; 41.85; 29.25.-t; 25.30.Bf

Keywords: Electron spectrometer; Magnetic spectrometer; Electron scattering; Targets; Magneto-optics

1. Introduction

Electron scattering experiments like those conducted at the Internal Target Facility [1,2] of NIKHEF require the determination of the energy and momentum transfer $(\omega, \boldsymbol{q})$ of the electron and, since extended targets are used, the position of the scattering vertex. In a preceding article [3] the newly constructed BigBite spectrometer, which provides this information, has been described. This spectrometer is characterized by a large solid angle (96 msr) combined with a very large momentum acceptance (200–900 MeV/c). The spectrometer consists of a single dipole magnet followed by a detector system which provides accurate timing

* Corresponding author. Tel.: + 31 20 592 2076; fax: + 31 20 592 5155; e-mail: josst@nikhef.nl.

0168-9002/98/$19.00
PII: S0168-9002(98)00476-8

($\sigma = 0.75$ ns) through the use of a fast scintillator, and tracking information by two sets of drift chambers separated by 700 mm. A diffusely reflecting, threshold Čerenkov detector provides discrimination between relativistic and non-relativistic particles. The resolution of the coordinate measurements in the drift chambers is about $\sigma = 150\,\mu$m in the dispersive direction, and about $\sigma = 100\,\mu$m [3] in the non-dispersive direction.

The design goal of the detector system is to achieve a momentum resolution for the scattered particle of $\sigma = 0.5\%$, a position resolution along the length of the target of 5 mm, and an angular resolution in both the scattering plane and the out-of-plane direction of 4 mrad. The coordinates at the target have to be obtained from the positions measured in the wire chambers with the help of backtracking techniques. In principle, the backtracking can be done by calculations based on a field map of the magnetic field. However, small misalignments of the components of the spectrometer introduce systematic errors. One may eliminate those by performing calibration experiments in which the direction and energy of the incoming particles are known [4]. From the measured positions in the detector package it is then possible to calculate the transfer coefficients (matrix elements) to perform the required backtracking calculations for actual experiments. This technique has successfully been employed for the QDD and QDQ spectrometers at NIKHEF using scattering off a thin ^{12}C foil and a so-called sieve slit [5,6]. For BigBite the use of a sieve slit is not appropriate. In internal target experiments at NIKHEF the target is an open-ended storage cell, filled with low-pressure hydrogen or helium gas [7]. This results in extremely thin targets. The sieve slit with narrow holes which are necessary to obtain a well-defined position, in combination with the large length of the interaction region, would result in extremely small values for the count rates. In addition, the non-focusing behaviour of BigBite would hamper the interpretation of the results.

For these reasons we have opted for a different approach. The calibration was performed in two steps. In the first experiment, in which a carbon rod was placed at the target position, the angle variables were determined. The beam of electrons in the storage ring was guided by means of steering magnets away from the rod, such that only a small fraction in the tail of its spatial distribution hit the target. The position of the scattered electron was measured by an additional wire chamber placed in front of the magnet. The geometrical variables were reconstructed for two different vertex positions and within the full energy range. In a second experiment, coincidence measurements were performed on helium and hydrogen isotopes in which also the momentum of the scattered electron could be calculated. This allowed calibration of the measurements of this variable by the BigBite spectrometer. The use of a long gas target also allows to optimize the reconstruction of the geometrical variables for the full range of vertex positions. The experimental setup is described in Section 2. In Section 3 the coordinate systems are defined and the transformation from detector to target coordinates is treated. The results achieved with this spectrometer form the subject of Section 4.

2. Experimental details

The transfer coefficients are easily obtained when a dataset is available in which, for each event, the target variables and the corresponding positions and angles at the location of the detector are measured. Because of the large acceptance of the spectrometer in momentum, in solid angle, and in the position of the scattering vertex, such a dataset should be very large, and thus is time-consuming to obtain. The two-step process we have used employs a dedicated target and an extra wire chamber between the target and the spectrometer. In this section, the point-like targets and the multi-wire chamber used in the calibration are described.

2.1. Target

Several target configurations have been considered for the backtracking studies: a microfoil, a thin wire, and a thicker rod which is only grazed by the beam. In this section it will be shown that only the last of these is compatible with beam in the storage ring without destroying the target.

The introduction of a target in an electron storage ring causes a reduction of the lifetime of the beam in the machine through a number of mechanisms of which single (nuclear and electronic) scattering, multiple Coulomb scattering, and Bremsstrahlung are the most important. The effects of multiple and Møller scattering scale with the nuclear charge number Z. The single nuclear scattering scales with Z^2, but its contribution falls with energy and is small for typical electron energies in AmPS. The effect of Bremsstrahlung is energy independent and scales with $Z(Z+1)$. In Ref. [8] it is shown that the inverse lifetime of the beam, after correction for the lifetime in the empty ring, scales with $Z(Z+1)$, and therefore, the latter is the dominant mechanism. The lifetime was measured to be about 2 min for a ^{4}He-target with a thickness of 1×10^{15} atoms cm^{-2} [9]. The maximum permissible thickness for a carbon target is therefore 1.4×10^{14} atoms cm^{-2}. A 1 μm thick graphite foil (density $\rho\approx2$ g cm^{-3}) contains 1×10^{19} atoms cm^{-2} and reduces the lifetime of the beam to less than 1 ms. Therefore, the use of such a target is excluded.

A thin wire, which intercepts only a small fraction of the beam, might be used while maintaining a reasonable lifetime of the beam. The disturbing effect of such a target causes some beam particles to lose their synchronicity with the RF-system of the machine. This is counteracted by radiation damping with a characteristic time of 122 ms at an energy of 600 MeV [10]. When a particle interacts on an average less than once with the target within a damping time, the loss of the particle may be prevented. However, in this case the heat generated by the interaction of the beam with the wire ($\dot{Q}_{\mathrm{beam}}$) outstrips the cooling ($\dot{Q}_{\mathrm{cool}}$) causing damage to the wire. The heating by the beam is caused by energy loss processes (660 keV mm^{-1} per electron for carbon), and can be estimated assuming a Gaussian beam profile:

$$\dot{Q}_{\mathrm{beam}} = 660\,(I_0/e)\,d_{\mathrm{eff}}\ \mathrm{erf}(d_{\mathrm{eff}}/2\sigma_x), \tag{1}$$

where d_{eff} is the effective diameter of the target wire (mm), I_0 the beam current (mA), and σ_x the horizontal size of the beam (0.25 mm at the target in the case of AmPS). The heat generated $\dot{Q}_{\mathrm{beam}}$ is then given in electron volts. The error function, erf, is used to calculate the fraction of the beam intercepted by the target. In a wire with a diameter of 5 μm the heat load is about 3 W at a beam current of 100 mA.

The most important cooling mechanism in vacuum is radiation. Sublimation of graphite at $T_{\mathrm{subl}}=3640$ K occurs before melting. The maximum power lost by radiation can then be calculated from

$$\dot{Q}_{\mathrm{cool}} = \pi d\,10\sigma_y\,\varepsilon\sigma\,(T^4_{\mathrm{subl}} - T^4_{\mathrm{room}}), \tag{2}$$

where d is the diameter of the wire (mm), σ_y the vertical size of the beam (0.25 mm in the case of AmPS), ε the emissivity of the target (0.4), and σ the Stefan–Boltzmann radiation constant (5.67×10^{-14} W mm^{-2} K^{-4}). The factor 10 takes into account some spreading of the region of high temperature by conduction. The heat lost by radiation is only about 150 mW at the highest permissible temperature, much less than the 3 W heating power found above. This excludes the use of a thin wire in the beam to implement a localized target for the calibration of the spectrometer.

The energy available for heating the target can be reduced by making sure that the same beam-particle can only pass once through the target. This can be done through the use of a thick target. The amount of energy deposited in the target is then limited by the short time it takes to lose all the current from the machine. The total energy in this case is

$$W = 660\,(I_0/e)\,d\,\tau_0, \tag{3}$$

where τ_0 is the revolution time in AmPS (700 ns). This energy is limited for example to about 90 mJ for a 2 mm thick target and causes a temperature rise of only about 100 °C. In order to obtain a reasonable lifetime of the beam only a very small fraction of the current may pass through the target. This can be achieved by skimming the target at a safe distance, which may gradually be decreased during the lifetime of the beam to keep the intercepted current approximately constant. The design of AmPS allows the application of a local displacement of the beam in the target region [10], which is needed for this technique.

Therefore, the target is made of two 2 mm diameter rods of graphite, mounted at a distance from

the closed orbit of 1 and 3 mm, respectively, displaced towards the centre of the storage ring. One rod is mounted on the axis of rotation of the spectrometer, the other 15 cm downstream from that. During injection the beam is steered about 7 mm away from the centre of the ring, clear of the target. When the beam is damped to its closed orbit, the distance to the target is reduced to about 2.5 mm to achieve a lifetime of the beam of a few minutes, and a count rate in the BigBite detectors of a few hundred events s^{-1}.

2.2. Vertex chamber

For the calibration experiment a multi-wire proportional chamber with a sensitive area of $32 \times 64\,cm^2$ was mounted between the target and the entrance of the BigBite spectrometer. The chamber determines, together with the target position, the track of the particle before the magnet. It consists of two planes; the sense wires are strung at a pitch of 2 mm in both the horizontal and vertical directions. The vertical wires are connected individually to the read-out electronics, the horizontal wires are first grouped in pairs. Only the central $16 \times 60\,cm^2$ of the chamber was instrumented. The electronics determines which wires have a signal within a 30 ns window around the event as defined by the spectrometer. The start and duration of this window can be adjusted to accommodate the full range of drift times. The chamber is operated at a high voltage of -3350 V applied to the cathode foils, and is flowed with a mixture of argon and isobutane in a ratio of 2:1 in volume. A more detailed description can be found in Ref. [11].

The MWPC is mounted at a distance of 65 cm from the target, perpendicular to the central ray through the BigBite spectrometer. Its position is fixed with two dowel pins. The angular resolution provided by the combination of target and MWPC is therefore, given by the wire pitch and amounts to 3 mrad ($\sigma = 0.9$ mrad) in the horizontal, and 6 mrad ($\sigma = 1.8$ mrad) in the vertical direction. In actual experiments with BigBite, this chamber is removed to avoid the multiple scatter it causes.

3. Calculation of target coordinates

The central ray is defined to be the trajectory of a particle in the symmetry plane of the magnet, starting at the centre of the target in the direction perpendicular to the entrance face of the magnet and in the magnet is bent with a radius R through an angle α. For the BigBite spectrometer these construction parameters are $R = 1.81$ m and $\alpha = 25^\circ$. A curvi-linear coordinate system is defined everywhere along this trajectory with its z-axis directed along the central ray, the x-axis in the symmetry plane pointing away from the centre of curvature, and the y-axis directed to make a right-handed system. Two special instances of this coordinate system will be used in this section. The first has its origin, O_t, at the centre of the target and the second with its origin, O_d, in the detection plane. The detection plane is defined to be the plane through the sense wires of the first half of the first drift chamber. Cartesian angles θ and ϕ are defined to be the angles with the z-axis in the xz-and yz-planes, respectively. This section describes the transformation from the coordinates measured in the detection plane $(x_d,\theta_d,y_d,\phi_d)$ to the target coordinates $(p_t,\theta_t,y_t,\phi_t)$, where p_t is the momentum of the particle.

The coordinates at the target have to be obtained from the measured position and direction of the track of the particle behind the magnet with the help of backtracking techniques. In principle, the backtracking can be done numerically by calculations based on a (measured) field map of the magnetic field. This would, however, entail a prohibitively large demand on computer time when done on an event by event basis. In addition small misalignments of the spectrometer components introduce systematic errors, which are difficult to correct for. Another method is to write any target quantity H_t as a polynomial in the detector-plane coordinates [12],

$$H_t = \sum_{i,j,k,l} a_{i,j,k,l}\, x_d^i \theta_d^j y_d^k \phi_d^l. \tag{4}$$

In the case of focusing spectrometers with relatively small opening angles, the degree of these polynomials and the sum of i,j,k,l is small (3 or 4)

and many of these elements are zero [5,6]. BigBite is a non-focusing spectrometer and has large acceptances; therefore, many coefficients are needed. These could be obtained by performing a calibration experiment in which the position and energy of the incoming particles is correlated with known values for the target variables. The large number of coefficients makes this a difficult venture. We opted for a third method. In a first step, the backtracking is performed analytically, using a simplified model of the spectrometer. The result of this calculation is then corrected by adding a contribution of the type given by Eq. (4). In this case, the number of coefficients needed is much lower, and they can easily be obtained in a calibration experiment.

3.1. Dispersive coordinates

In the dispersive plane, the detector coordinates x_d and θ_d are measured. The target coordinates p_t and θ_t are closely associated with these variables. The first step in the determination of the target variables is the analytical calculation of these coordinates in a simplified model of the spectrometer. Fig. 1 shows a view of the dispersive plane. The field of the magnet is assumed to be homogeneous between the poles and zero outside this domain. The fringing fields are accounted for by extending this region slightly. In Fig. 1, the resulting effective field boundaries are indicated by the dotted lines. The track of the particle, as measured by the wire chambers, is traced back to the backward field boundary. Inside the magnet, the trajectory follows an arc of a circle which intersects the forward field boundary from where a straight path leads to the target. The condition that both straight sections of the trajectory are tangential to the arc is sufficient to calculate the position of the centre and the size of the radius of the circle. This trajectory is approximated by tracing the track from the wire chambers to the centre line of the magnet and connecting the intersection with the target point (see Fig. 1). That this yields a good first order description is illustrated in Fig. 2a, where the correlation is shown between the calculated angle θ_t and the angle θ_{vertex} observed by the vertex chamber. The remaining differences (RMS value 14.1 mrad) are minimized by adding corrections of the type given in Eq. (4). It is sufficient to apply only first and second order corrections, i.e. $i+j+k+l \leqslant 2$. Fig. 2b shows the same correlation after this correction; the resulting RMS value is 6.1 mrad.

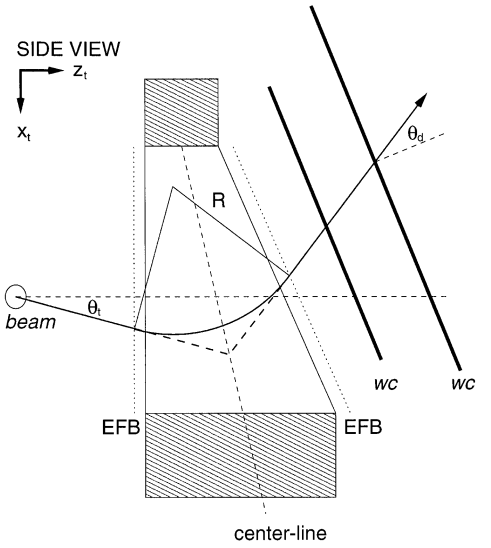

Fig. 1. View of the dispersive plane of the BigBite spectrometer. The dotted lines labelled EFB indicate the effective field boundaries. The position of the wire chambers is indicated by *wc*.

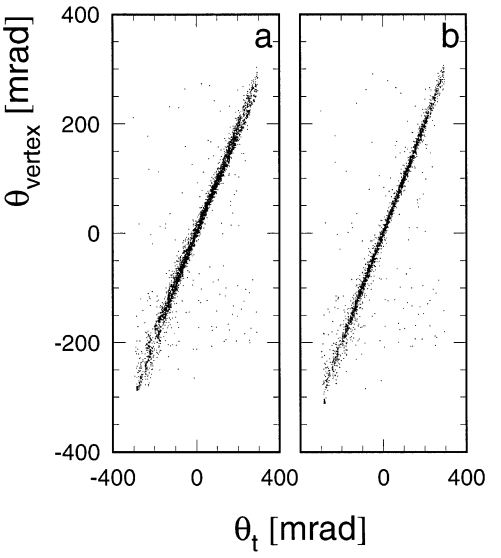

Fig. 2. Correlation of the measured angle θ_{vertex} of the track of the particle and the angle θ_t as obtained from the BigBite spectrometer. Panel (a) shows the result after the first, analytical, step. Panel (b) shows the result after the corrections of the type given in Eq. (4).

3.2. Non-dispersive coordinates

If a charged particle enters a region with a uniform magnetic field at right angles to its edge, no deflection will occur in the non-dispersive plane. However, when the trajectory is not perpendicular to this edge, a small angular deflection in the non-dispersive direction will result. This deflection was calculated by Penner [13] to be

$$\Delta\phi = -(y/R)\tan\beta, \tag{5}$$

where β is the angle of the projection of the trajectory on the symmetry plane of the magnet with the normal on the effective field boundary, y is the distance to this symmetry plane, and R is the radius of curvature of the track of the particle. The effect on leaving the field region is the same, but has the opposite sign. Fig. 3 shows a projection of a track on the yz-plane, where the two deflections are clearly visible. The first estimate of the angle ϕ_t is easily calculated by adding the two deflections according to Eq. (5) to the angle ϕ_d as determined by the wire chamber data. The correlation between this angle and the angle ϕ_{vertex} is used to further refine the calculation by adding, as in the case of θ_t, corrections of the type given in Eq. (4).

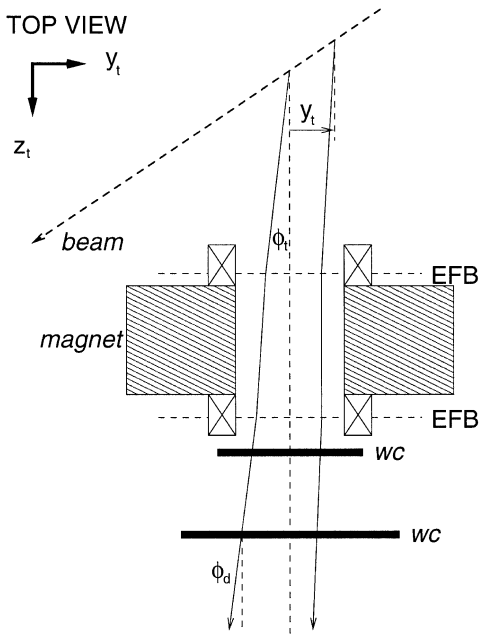

Fig. 3. View of the non-dispersive plane of the BigBite spectrometer. The position of the wire chambers is indicated with *wc*.

The displacement in the y-direction is calculated for each of the three segments of the trajectory by multiplying the lengths of these segments with the appropriate factor $\tan\phi$. The vertex position y_t, finally, is obtained by adding these displacements to the position y_d determined by the wire chambers. A data set with two target rods at two different positions along the beamline, and thus two different values for y_t, was used to determine corrections of the same type as those used for θ_t and ϕ_t.

3.3. Momentum

In Section 3.1, the first step has been described. The result for the radius R obtained in this step is used to determine the initial estimate of the momentum p_t. Corrections of the type given in Eq. (4) are added to this result in the second step. The data sets are obtained in the experiments in which the elastically scattered electron is measured in coincidence with the recoil nucleus, the momentum and identity of which were determined by the Recoil detector [14]. The elastic events are identified by the known correlations between kinematical variables. The momentum of the scattered electron can be calculated from the same relations. We used the elastic ^{4}He(e,e′α), ^{3}He(e,e′τ), and ^{1}H(e,e′p) reactions over a wide range of incident electron energies.

4. Results

The resolutions for p_t,θ_t,y_t, and ϕ_t of the BigBite spectrometer were determined in two different experiments. The first experiment used single-arm ^{12}C(e, e′) scattering from the target described in Section 2.1, while the second consisted of coincidence measurements using the elastic ^{4}He(e, e′α), ^{3}He(e, e′τ), and ^{1}H(e, e′p) reactions with a gas target. The geometrical variables (θ_t, ϕ_t, and y_t) could be compared to the data from both experiments, while p_t was accessible only in the last one.

4.1. Angular coordinates

The direction of the track leaving the target was determined using the vertex detector (see Section 2.2) and the known position of the target. The position of the vertex detector was fixed with respect to the magnet of the BigBite spectrometer which, in turn, was surveyed relative to the target point. The uncertainty in the alignment was estimated to be less than 0.1 mm, except for the horizontal position of the vertex chamber. No precision marks were available for the location of the vertical wires, therefore, this position was derived from data taken with the magnet switched off. The (vertical) position of the beam has been obtained from the control system of the AmPS ring. The estimated uncertainty in this position is 2 mm but its stability is much better. The beam position and its RMS-variation have been studied using a laser Compton scattering technique [15]. The variation in the beam position between fills, and within fills at different beam-currents, was found to be 30 μm [16], which is close to the precision of the method.

Fig. 4 shows the distribution of the differences between the angular coordinates at the target calculated from the spectrometer and the results obtained from the vertex chamber. The resolution of the spectrometer is estimated from these plots by taking the widths of the distributions and subtracting in quadrature the contribution from the vertex chamber (0.9 and 1.8 mrad in the horizontal and vertical directions, respectively, see Section 2.2). The introduction of the vertex chamber (thickness 0.09% of a radiation length) in the path of the particle introduces an additional contribution to the multiple scattering. This contribution (< 1 mrad) was subtracted from these values. Fig. 5 shows these resolutions (widths) as a function of the energy of the scattered electron. The resolution shows, apart from a constant term, a contribution which depends on $1/E$ as expected for multiple scattering inside the spectrometer. Note that in the case of the single-arm experiment any scattering which occurs close to the target (e.g. in the cell wall and in the window of the scattering box) can be ignored. The direction of the track is changed, but both the vertex chamber and the BigBite spectrometer measure the direction of the track after the scattering, and thus no correction is necessary in the comparison of these results.

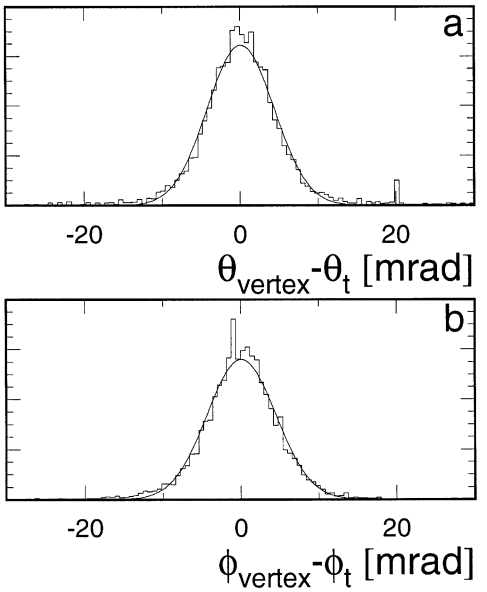

Fig. 4. Distributions of $\theta_{\text{vertex}} - \theta_t$ and $\phi_{\text{vertex}} - \phi_t$.

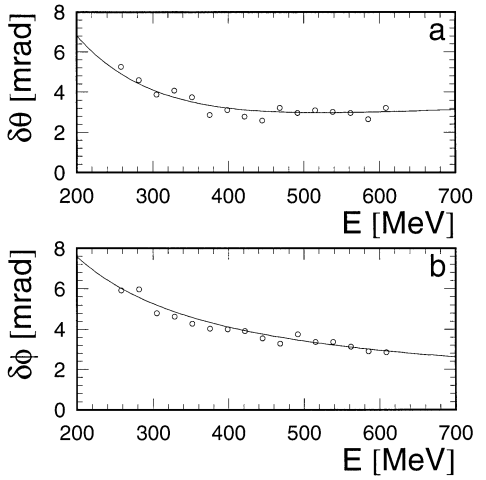

Fig. 5. Resolutions of θ_t and ϕ_t as a function of energy of the detected electron. The widths were corrected for the contribution from the multiple scattering caused by the vertex chamber.

The different energy dependence of the θ_t and ϕ_t resolution is caused by the different coefficients

linking θ_t to θ_d and ϕ_t to ϕ_d, respectively. The leading term for θ_t is $\theta_t = -0.63\,\theta_d + \cdots$, while $\phi_t = \phi_d + \cdots$. Thus, the effects of multiple scattering in the air in the flight path and the foils of the MWDCs are reduced for θ_t, but remain present in full for ϕ_t.

In a separate experiment, the same angles were determined in the kinematically over-complete elastic ^{4}He(e,e′α) reaction. For the detection of the recoiling ^{4}He-nucleus the recently developed Recoil detector was employed [14]. The laboratory coordinate frame is used with its origin at the centre of the target which coincides with the axis of rotation of the BigBite spectrometer. The z-axis in this system points in the direction of the electron beam, the x-axis is in the plane of the AmPS ring pointing outward, and the y-axis points up to make a right-handed system. Polar angles θ_{lab} and ϕ_{lab} are defined in the usual way. The Cartesian angles θ_t and ϕ_t can be expressed in the laboratory frame in the following way:

$$\tan\theta_t = \frac{-y_{lab}}{\sqrt{x_{lab}^2 + z_{lab}^2}} = \frac{-\sin\theta_{lab}\sin\phi_{lab}}{\sqrt{\cos^2\theta_{lab} + \sin^2\theta_{lab}\cos^2\phi_{lab}}},$$

$$\tan(\theta_{BB} + \phi_t) = x_{lab}/z_{lab} = \tan\theta_{lab}\cos\phi_{lab}, \qquad (6)$$

where θ_{BB} is the angle between the optical axis of the spectrometer and the beam.

The direction of the scattered electron in this frame is described by the following equations. Both scattered particles and the beam are within a single plane, therefore

$$\phi^{\alpha}_{lab} - \phi^{e'}_{lab} = \pi. \qquad (7)$$

The scattering angle of the electron can be calculated from the energy of the recoiling α-particle

$$\sin\tfrac{1}{2}\theta^{e'}_{lab} = \sqrt{\frac{m_\alpha T_\alpha}{2E_0(E_0 - T_\alpha)}}, \qquad (8)$$

where E_0 is the initial electron energy and m_α the mass of the recoiling nucleus. The kinetic energy of the α-particle can be determined precisely ($\delta T_\alpha = 0.1$ MeV [14]) and the energy spread of the stored beam ($\delta E_0/E_0 = 1\times10^{-4}$ [17]) is small. Fig. 6 shows the distributions of the deviations of the measured angles, converted to the laboratory frame, from the calculated ones. The peaks are not centred around zero, showing the effect of systematic errors. The offset in the azimuthal angle is caused by the non-zero y-coordinate of the beam. The effect of a 1 mm offset of this position is $+6$ mrad in ϕ^{α}_{lab} and -1.3 mrad in $\phi^{e'}_{lab}$. The observed peak position in Fig. 6a can be attributed to a misalignment of -1.4 mm in the beam height, which was not independently measured. The systematic error in the scattering angle is dominated by the uncertainty in the absolute value of E_0. In the injection process, a small change ($< 0.8\%$) of the electron energy in the downward direction is allowed to ease the capture of the beam from the linac (RF-frequency 2856 MHz) into the AmPS ring (RF-frequency 476 MHz). This affects the determination of $\theta^{e'}_{lab}$, which will shift -1 mrad MeV^{-1}. If the observed deviation from zero (-3 mrad) in the peak position in Fig. 6b is caused fully by the error in the absolute value of E_0, this would mean a 3 MeV lower energy, which is within the range mentioned above. A second contribution stems from a possible misalignment of the vertex chamber during the calibration, which will effect θ_{lab}. This is inextricably mixed with the former but is estimated to be smaller.

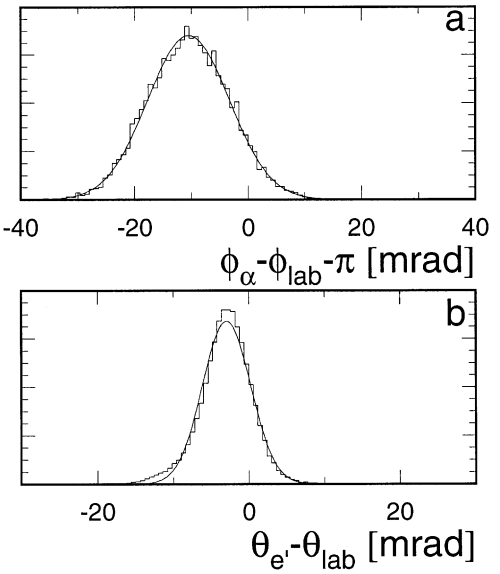

Fig. 6. Distributions of $\phi^{\alpha}_{lab} - \phi_{lab} - \pi$ and $\theta^{e'}_{lab} - \theta_{lab}$.

The angles θ_t and ϕ_t have a limited range determined by the solid angle of the spectrometer. In this range, Eq. (6) can be approximated by

$$\theta_t \approx -(\sin\theta_{BB})\phi_{lab},$$

$$\phi_t \approx \theta_{lab} - \theta_{BB}. \quad (9)$$

The resolution in θ_t is derived from Fig. 6a. The distribution of $\phi^{\alpha}_{lab} - \phi_{lab} - \pi$ has a width $\sigma = 7.26$ mrad. The resolution of the Recoil detector in this direction is given by the width of the horizontal silicon strips (3.14 mm) and the distance of the Recoil detector to the centre of the target (17 cm). It amounts to $\sigma = 5.33$ mrad. The resolution in θ_t is calculated from Eq. (9) using the position of the BigBite spectrometer ($\theta_{BB} = 30^\circ$) with the resulting width of $\sigma = 2.5$ mrad. In the other direction, the resolution is obtained from Fig. 6b ($\sigma = 3.20$ mrad) corrected for the uncertainty introduced by the calculation of $\theta^{e'}_{lab}$ ($\sigma = 2$ mrad). The result in this direction is also $\sigma = 2.5$ mrad. These values still contain a contribution from multiple scattering in the target cell and the exit window of the scattering box (1 mrad). After correction for these contributions, the angular resolution of BigBite is found to be 2.3 mrad. This value is close to the value obtained with the resolutions as determined by means of the vertex detector (3.0 mrad at 600 MeV for θ_t and ϕ_t, see Fig. 5). The slightly better resolution as determined in the coincidence experiment is caused by the fact that, in this case, only a limited part of the acceptance of BigBite has been exploited, while in the single-arm data, the full acceptance was used. Analyzing the same data as in Fig. 5, but restricting the acceptance to a region similar as that used in the coincidence measurements, reproduced the 2.3 mrad result.

4.2. Vertex position

The resolution in the determination of the vertex position was measured in two ways. First, the single-arm ^{12}C(e,e′) data were used. In this experiment, the target consisted of two carbon rods mounted close to the beam 15 cm apart (see Section 2.1). The known positions of the rods ($z = 0$ and $z = +15$ cm in the laboratory frame) are expressed in BigBite coordinates ($y_{rod} = 0$ and $y_{rod} = 15 \sin\theta_{BB}$ cm). The difference between the values calculated from the BigBite information y_t and y_{rod} is shown in Fig. 7a. The width of the distribution is $\sigma = 0.5$ cm. The second panel in Fig. 7 shows the resolution δy_t as a function of the detected electron energy. The results can be described by a constant term ($\delta y_t = 0.3$ cm) and a contribution due to multiple scattering which is proportional to $1/E$. The influence of the vertex chamber on these results is negligible and has not been corrected for.

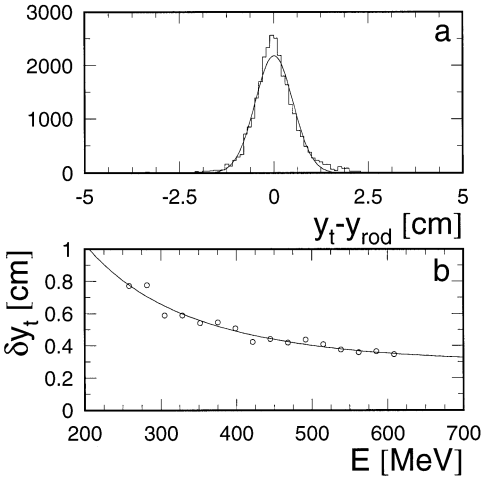

Fig. 7. (a) Distribution of $y_t - y_{rod}$. (b) The width of this distribution as a function of the energy of the detected electron.

In the coincidence experiment, the location of the scattering vertex can be determined by the Recoil detector. The direction of the recoiling nucleus can be determined from other kinematical variables through the following formula:

$$\cos\theta_\alpha = \frac{T_\alpha(E_0 + m_\alpha)}{E_0\sqrt{2m_\alpha T_\alpha + T_\alpha^2}}. \quad (10)$$

The angle θ_α is determined by the energy E_0 and the energy T_α determined by the Recoil detector. The position of the vertex is determined by this angle and the locus of the hit on the Recoil detector. Using the same uncertainties in E_0 and T_α as before, the error in the calculated position (z_α) of the scattering vertex is 1 mm. Fig. 8 shows the distribution of the difference between the position calculated using the BigBite data (z_{lab}) and z_α. The

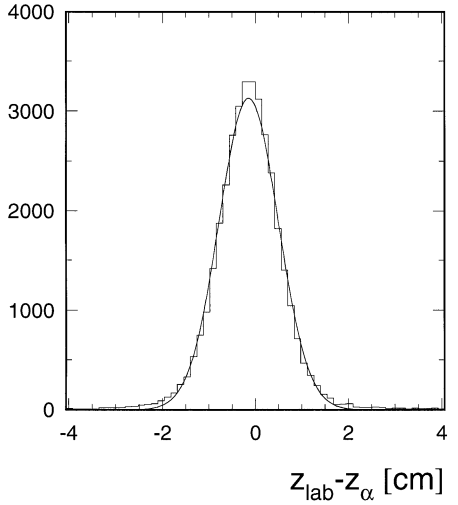

Fig. 8. Distribution of $z_{lab} - z_\alpha$.

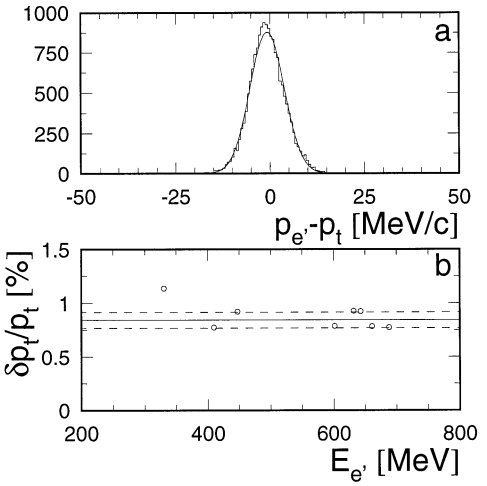

Fig. 9. (a) Distribution of $p_{e'} - p_t$ in the measurements of elastic scattering off ^{4}He. The energy of the incident electrons was 615 MeV. (b) Resolution $\delta p_t/p_t$ as a function of the energy of the scattered electron.

width of this distribution is $\sigma = 6.4$ mm. The resolution of the BigBite spectrometer in the y_t coordinate is obtained by multiplying the width of this distribution, corrected for the uncertainty in z_α, by $\sin\theta_{BB}$ with the result $\sigma = 3.2$ mm. This value is the same as that obtained from Fig. 7b for $E' = 600$ MeV.

4.3. Momentum determination

The resolution in the momentum measurement of the spectrometer has been determined in the coincidence experiment. The recoiling nucleus was detected with the Recoil detector and the elastic scattering process was used for which the missing energy $E_m = E_0 - E_{e'} - T_\alpha$ is zero. The momentum of the scattered particle can be calculated from this formula with the result in the case of an electron,

$$p_{e'} = (E_0 - T_\alpha)/c. \tag{11}$$

The width of the measured distribution of $p_{e'} - p_t$ is a measure of the resolution in the experiment, which is dominated by that of the electron spectrometer. Fig. 9a shows a result at an incident energy of 615 MeV. The width of this distribution is $\sigma = 4.74$ MeV/c. Fig. 9b shows the resolutions $\delta p_t/p_t$ at a few different energies. The mean value is $\sigma = 0.84\%$, with a standard deviation of 0.07%.

5. Summary

The BigBite spectrometer has been shown to operate in electron scattering experiments at the Internal Target Facility of the AmPS storage ring at NIKHEF. It has been calibrated using a two-step approach in which a first analytical approximation was followed by a second step where corrections to the former were applied using a method inspired on the matrix method. The angular resolution of the spectrometer was found to be 3 mrad in θ_t and ϕ_t at about 600 MeV, using the full acceptance of the spectrometer. The resolution deteriorates slightly at lower energies due to multiple scattering in the flight path and the wire chambers. These values have been corrected for contributions caused by multiple scattering in the target and other materials in front of the entrance to the spectrometer which were present during the calibration experiments. The position of the vertex can be determined with a resolution of 3.2 mm at 600 MeV, again deteriorating somewhat towards lower energies as a result of multiple scattering.

Finally, the momentum resolution was found to be 0.84%. This latter result is slightly higher than the design value of 0.5%, while the observed geometrical resolutions (angles and vertex position) are better than the design goals.

Acknowledgements

The design and construction of the Čerenkov detector was a part of the research supported by DOE grant DE-FG05-87ER40364 and the University of Virginia. This work was supported in part by the Stichting voor Fundamenteel Onderzoek der Materie (FOM), which is financially supported by the Nederlandse Organisatie voor Wetenschappelijk Onderzoek (NWO).

References

[1] K. de Jager, Recent results from the NIKHEF internal target program, in: S. Boffi et al. (Eds.), Proc. Conf. on Perspectives in Hadronic Physics, ICTP, Trieste, 12–16 May, 1998, World Scientific, Singapore, pp. 1–10.
[2] J.F.J. van den Brand, Electron scattering from polarized internal targets at AmPS, in: C.W. de Jager et al. (Eds.), Spin96 Proc., World Scientific, Singapore, 1997, pp. 149–160.
[3] D.J.J. de Lange et al., Nucl. Instr. and Meth. A 406 (1998) 182–194.
[4] H. Blok et al., Nucl. Instr. and Meth. A 262 (1987) 291.
[5] E.A.J.M. Offermann et al., Nucl. Instr. and Meth. A 262 (1987) 298.
[6] L. deVries et al., Nucl. Instr. and Meth. A 292 (1990) 629.
[7] Z.-L. Zhou et al., Nucl. Instr. and Meth. A 378 (1996) 40.
[8] T. Botto et al., in: H.P. Schieck, L. Sydow (Eds.), Int. workshop on Polarized beams and polarized gas targets, World Scientific, Singapore, 1996, pp. 382–387.
[9] D.J.J. de Lange, Ph.D. Thesis, University of Utrecht, 1998, unpublished.
[10] Wu Yunyan, Ph.D. Thesis, Technical University of Eindhoven, 1991, unpublished.
[11] S. Choi, M.Sc. Thesis, Arizona State University, 1994, unpublished.
[12] W. Bertozzi et al., Nucl. Instr. and Meth. A 162 (1979) 211.
[13] S. Penner, Rev. Sci. Instrum. 32 (1961) 150.
[14] M.J.M. van Sambeek, Ph.D. Thesis, Free University of Amsterdam, 1997, unpublished.
[15] R. Tamoschat et al., Emittance measurement at the Amsterdam Pulse Stretcher, in: A. Ghigo, M. Giabbai, G. Possamza (Eds.), Proc. 3rd European workshop on beam diagnostics and instrumentation for particle accelerators, 1997, LNF-Report 97048, p. 144.
[16] R. Tamoschat, private communication.
[17] P.K.A. de Witt Huberts, Nucl. Phys. A 553 (1993) 845c.